

Songbird connectome reveals tunneling of migratory neurons in the adult striatum

Shvedov, N.R.^{1,2}, Castonguay, S.J.³, Rother, A.⁴, Schick, D.E.⁴, Kornfeld, J.^{4,5}, Scott, B.B^{2,3,6,7}

¹ Graduate Program in Neuroscience, Boston University, Boston, MA, USA

²Center for Neurophotonics, Boston University, Boston, MA, USA

³ Psychological & Brain Sciences, Boston University, Boston, MA, USA

⁴ Max Planck Institute for Biological Intelligence, Martinsried, Germany

⁵ MRC Laboratory of Molecular Biology, Cambridge Biomedical Campus, Cambridge UK

⁶ Center for Systems Neuroscience, Boston University, Boston, MA, USA

⁷ Correspondence: bbs@bu.edu

15 **Abstract**

16 Immature neurons in the adult brain migrate and integrate into existing circuits, where they
17 contribute to plasticity, learning, and complex behaviors. However, how these cells navigate
18 synapse-rich regions of the adult brain remains poorly understood. While prior studies have
19 examined the molecular mechanisms and functional consequences of adult neurogenesis, few
20 have investigated the physical interactions between migrating neurons and their surrounding
21 environment. Here, we use electron microscopy-based connectomics to examine how migrating
22 neurons interact with mature circuit elements in the adult zebra finch striatum. Immature neurons
23 exhibiting migratory features were observed contacting diverse structures in their
24 microenvironment, including the axons, dendrites, synapses, and somas of mature neurons.
25 Surprisingly, these interactions were structurally complex, often involving pronounced
26 deformations of mature somas and the surrounding neuropil. These deformations appeared as
27 “tunnels” made by the migratory neurons as they displaced mature structures along their path.
28 Together, these findings suggest that migrating neurons may physically reshape the mature circuit
29 to reach their targets, revealing an unexpected degree of structural and functional plasticity in the
30 adult brain.

31 **Introduction**

32 Adult neurogenesis is believed to play an important role in learning and memory, tissue
33 homeostasis, and regeneration^{1–3}. In many adult vertebrates, this process involves migration, in
34 which immature neurons move from proliferative zones to their integration targets. Mature brain
35 tissue poses several challenges for migrating neurons. Compared with the developing brain, adult
36 brains have increased cell density and diminished extracellular space⁴, and are rich in stable
37 synapses, believed to form the basis of behavior and long-term memory^{5,6}. Given these
38 constraints, how migratory neurons can physically navigate through the adult brain environment
39 is not clear.

40 Songbirds are a valuable model organism for the study of neuron migration in the adult
41 brain^{7,8}. In these species, new neurons integrate into brain regions that control complex learned
42 behaviors, where they establish synapses with mature neurons and respond to sensory stimuli^{9–}
43 ¹³. New neurons are added to at least two subregions within the circuit that control learning and
44 production of song--HVC, a pallial premotor nucleus, and Area X, a region within the striatum¹⁴.

45 New neurons that migrate to the striatum are born within a region of the lateral ventricle,
46 corresponding to the mammalian medial ganglionic eminence (MGE)^{15,16}. After arrival in the
47 striatum, they differentiate into medium spiny neurons (MSN) and integrate into the local circuit
48 ^{17–19}. New neurons have also been reported in the adult mammalian striatum^{20–22}, motivating
49 further study of neurogenesis in this region in songbirds. However, a key problem is how the new
50 neurons interact with mature circuit structures in the striatum, such as axons, dendrites, and
51 neuronal somas.

52 Here, we leverage the ultrastructural resolution and dense labeling of electron microscopy
53 (EM) connectomics to investigate the microenvironment of migratory neurons in the adult brain.
54 We focused on the first fully reconstructed zebra finch connectome, collected from the song
55 nucleus Area X in the striatum^{23,24}. Within this dataset, we identified a population of migratory
56 neurons using a supervised machine-learning classifier based on morphological features derived
57 from fluorescence microscopy. These cells had ultrastructural features consistent with migratory
58 neurons, like elongated nuclei, a centriole pair at the base of the leading process, and filopodia-
59 like extensions at the end of the leading process.

60 This rich dataset revealed several unexpected phenomena. Migratory neurons were
61 observed in a synapse-dense neuropil and made extensive contacts with various features of
62 mature neurons including spines, axons, and dendrites. Migratory neurons also made frequent
63 soma-soma contacts with mature neurons, which form large soma clusters in the avian striatum.
64 Interactions between new neurons and mature neurons were asymmetrical, with migratory
65 neurons deforming adjacent mature neurons and neuropil. In some instances, these indentations
66 were so extreme that the new neurons appeared to tunnel through the clusters of mature neurons.
67 These results reveal the value of applying EM connectomics to adult neurogenesis and suggest
68 that migratory neurons may dramatically perturb the existing functional circuits as they migrate
69 and integrate. Furthermore, they reveal the remarkable structural flexibility of mature neural
70 circuits.

71 **Results**

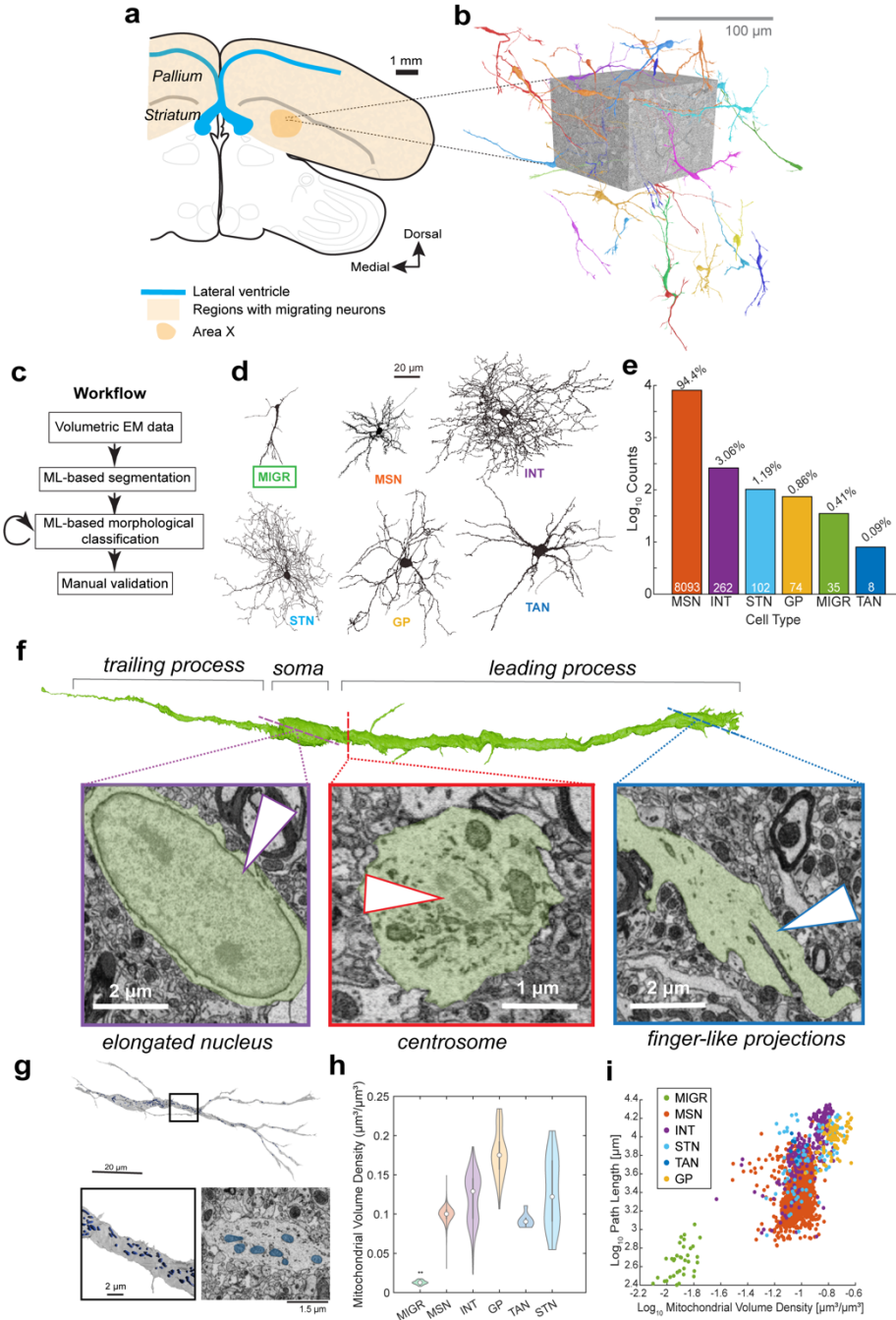
72 Migratory neurons identified by morphological and ultrastructural features in EM dataset

73 To identify migratory neurons in the songbird basal ganglia connectome²³ we created a
74 library of ground truth morphologies of new neurons in the striatum using fluorescence microscopy
75 in tissue sections (**Fig. S1**). We used transgenic songbirds in which new neurons are sparsely
76 labeled with GFP²⁵, allowing visualization of the cellular morphology, combined with
77 immunohistochemistry for doublecortin (DCX), a marker for migratory neurons^{26,27} or Hu to label
78 neuronal identity^{28,29}. These cells had two or more processes, and possessed a spindle-shaped
79 soma with a thinner “trailing” process behind the soma, and a thicker leading process in front of
80 the soma, which was often bifurcated (**Fig. S1,S2**). These cells resembled migrating neurons in
81 other regions of the adult avian forebrain³⁰ and in the developing mammalian brain^{31,32}.

82 We used a machine-learning based classifier, trained on a subset of manually identified
83 cells, to identify other migratory neurons from the dataset (**Fig. 1a-d; Fig. S1**; see **Methods**) This
84 approach defined a cell class consisting of 135 objects. Manual inspection revealed that 40
85 objects within this class met criteria for migrating neurons (false positives = 95/135; false
86 negatives = 0; see **Methods**). We selected 35 true positives with largely complete reconstructions
87 for further analysis (**Fig. S2**).

88 Identified cells had distinct morphological and ultrastructural features consistent with a
89 migratory neuron identity (**Fig. 1f**). All cells had an elongated soma with thin cytoplasm
90 surrounding a nucleus containing one or more nucleoli with heterochromatin-dense edges, as
91 reported previously for migratory neurons across species and developmental stages^{29,33-37}. In
92 34/35 of these cells, the centrosome was clearly located below the nucleus at the base of the
93 leading process, as expected for migratory neurons^{33,38,39}. A golgi apparatus was typically found
94 near the centrosome, which has been reported to be aligned with the direction of neuron migration
95 in immature neurons⁴⁰⁻⁴². All had one or more “finger-like” projections at the distal tips of their
96 leading processes, similar to the filopodia or growth-cone structures described for migrating
97 neurons and extending neurites⁴³. Finally, these cells typically had small, rounded mitochondria,
98 which were clustered around the centrosome, as previously described for immature and migratory
99 neurons^{44,45} (**Fig. 1g**). They also exhibited a significantly lower mitochondrial density than mature
100 neurons (**Fig. 1g-i**), perhaps indicative of a lower metabolic demand^{44,46-50}.

101 Together, our findings demonstrate that the songbird basal ganglia connectome²³ contains
102 a distinct class of cells with morphological and ultrastructural features that resemble immature
103 neurons in the midst of or in the end stages of migration.



104

Figure 1. Identification of migratory neurons in volumetric EM

105 A) Overview of neuron migration in adult zebra finch brain. Neurons are born in the ventricular wall (blue line), and migrate throughout the pallium and striatum (orange shading), including Area X (orange outline).
 106 B) Reconstructions of migratory neurons from volumetric EM. C) Workflow for automated identification of
 107 migratory neurons. D) Tracings of representative cells from identified cell classes. E) Prevalence for each
 108 cell class in the data set. F) Ultrastructural features (arrows) characteristic of migratory neurons from an
 109 example cell. G) (top) Reconstruction of migratory cell with segmented mitochondria in blue. (bottom left)
 110 Zoom in on box region from top panel. (bottom right). Zoom-in cross section with mitochondria in blue. H) Mitochondrial densities across cell types. MIGR cell type has significantly lower mitochondrial densities
 111 than all other cell types (one-way ANOVA, $p = 0$). I) Path lengths and mitochondrial density volume for
 112 immature and mature neuron classes.
 113

115 Migratory neurons are present at a high density and oriented in multiple directions

116 Next, we evaluated the orientations and positions of identified migratory neurons
117 throughout the connectome. We defined the orientation of the cell as a 3-dimensional vector
118 beginning at the soma and ending at the first branch point of the leading process (**Fig. S3a,b;**
119 **Methods**). Leading process vectors from different cells were oriented in a variety of directions
120 (**Fig. S3a,d**). No directional bias was detected in the horizontal plane (Rayleigh's test, $p = 0.05$)
121 and a slight bias was detected in the azimuth plane (Rayleigh's test, $p < 0.001$).

122 Identified migratory neurons were present at a density of 1,390 neurons per mm^3 (35 cells
123 in 0.025 mm^3) and their distribution in the volume was well fit by a maximum entropy model,
124 indicating uniform distribution throughout the tissue (**Fig. S3e**). Our findings of high soma position
125 entropy and multidirectional leading process orientation are similar to observations from *in vivo*
126 imaging studies of migration^{25,30} and consistent with a diffusion-like process.

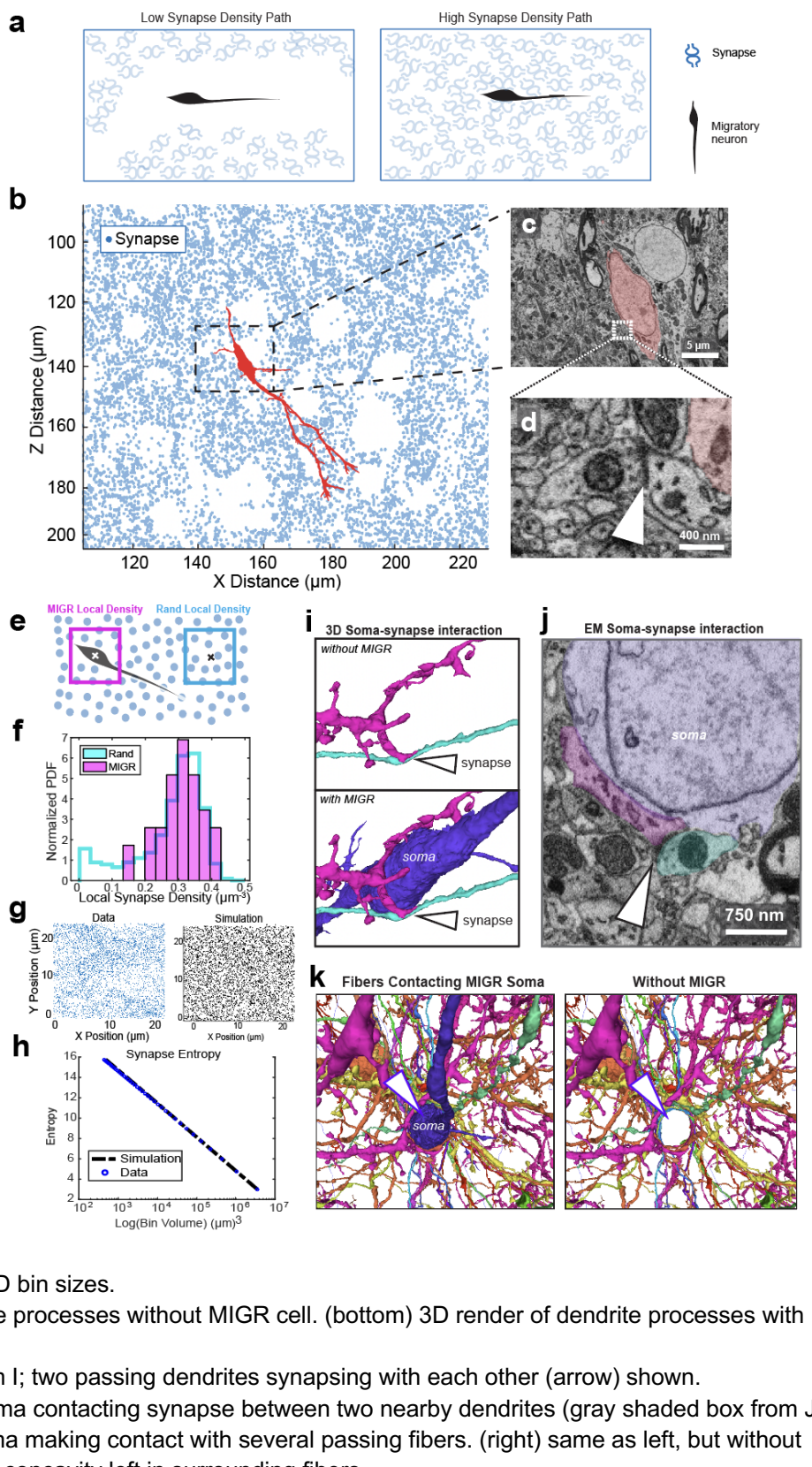
127 Migratory cells are located within synapse-dense neuropil

128 Since migratory neurons were widely distributed throughout the tissue volume, we
129 investigated whether they were located within regions rich in synapses, or, alternatively,
130 constrained to low synapse density corridors (**Fig. 2a**). This connectome contains over 8 million
131 high-confidence (>0.9 certainty) synapses at a density of 0.29 per μm^3 (**Fig. 2b-d**). The local
132 synapse density surrounding migratory neurons was not significantly different from the global
133 synapse density (0.31 ± 0.07 per μm^3 , one-sample t-test, $p = 0.12$) or the density of synapses
134 surrounding random points throughout the volume (0.28 ± 0.11 per μm^3 , Kolmogorov-Smirnov
135 test, $p = 0.35$, **Fig. 2e,f; Methods**), suggesting a roughly uniform probability distribution of
136 synapses throughout the tissue. Indeed, the distribution of synapses throughout the entire volume
137 was well fit by a maximum entropy model (uniform distribution, $n = 8,278,615$ simulated synapses)
138 (**Fig. 2g-h**).

139 Finally, visual inspection of ultrastructural features revealed that migratory neurons made
140 contact with mature synapses (**Fig. 2i,j**). Moreover, we observed dendrites of mature neurons
141 curving around the soma of migratory cells, raising the possibility that migratory neuron somata
142 deform neuropil in their vicinity. Together, these findings suggest that new neurons are not
143 preferentially migrating through low-synapse-density corridors, and instead migrate through
144 neuropil highly dense in synapses.

145 **Figure 2. Migratory cells located within synapse-dense neuropil**

- 146 A. Conceptual models:
 147 neurons may migrate
 148 through channels with low
 149 numbers of synapses (left)
 150 or through areas of high
 151 synapse density (right).
 152 B. Synapse locations (blue)
 153 surrounding a migratory
 154 neuron (MIGR) cell (red).
 155 C. Electron micrograph of
 156 dashed box in B.
 157 D. Zoom in on the dashed
 158 box region in C, showing
 159 synapse (arrow) near
 160 MIGR soma (red).
 161 E. Schematic for local density
 162 computation method.
 163 F. Histogram of local
 164 densities around MIGR
 165 cells ($n = 35$) and random
 166 points ($n = 29484$). No
 167 significant difference was
 168 found between local MIGR
 169 density and local Rand
 170 density (K-S test, $p =$
 171 0.35).
 172 G. (left) Synapse coordinate
 173 data in $25 \mu\text{m} \times 25 \mu\text{m} \times$
 174 $10 \mu\text{m}$ FOV (confidence \geq
 175 0.9; $n = 4929$ synapses).
 176 (right) Simulated synapse
 177 coordinates in $25 \mu\text{m} \times 25$
 178 $\mu\text{m} \times 10 \mu\text{m}$ FOV ($n =$
 179 4929 simulated synapses).
 180 The simulation assumed a
 181 maximum entropy model
 182 and followed a uniform
 183 probability distribution.
 184 H. The Shannon Entropy of
 185 the synapse coordinates
 186 vs simulated uniform
 187 distribution across varying 3D bin sizes.
 188 I. (upper) 3D render of dendrite processes without MIGR cell. (bottom) 3D render of dendrite processes with
 189 MIGR cell.
 190 J. Zoom in on MIGR soma from I; two passing dendrites synapsing with each other (arrow) shown.
 191 K. EM micrograph of MIGR soma contacting synapse between two nearby dendrites (gray shaded box from J).
 192 L. (left) 3D render of MIGR soma making contact with several passing fibers. (right) same as left, but without
 193 MIGR visualization, showing concavity left in surrounding fibers.



194 Migratory neurons interact with mature neuron somas

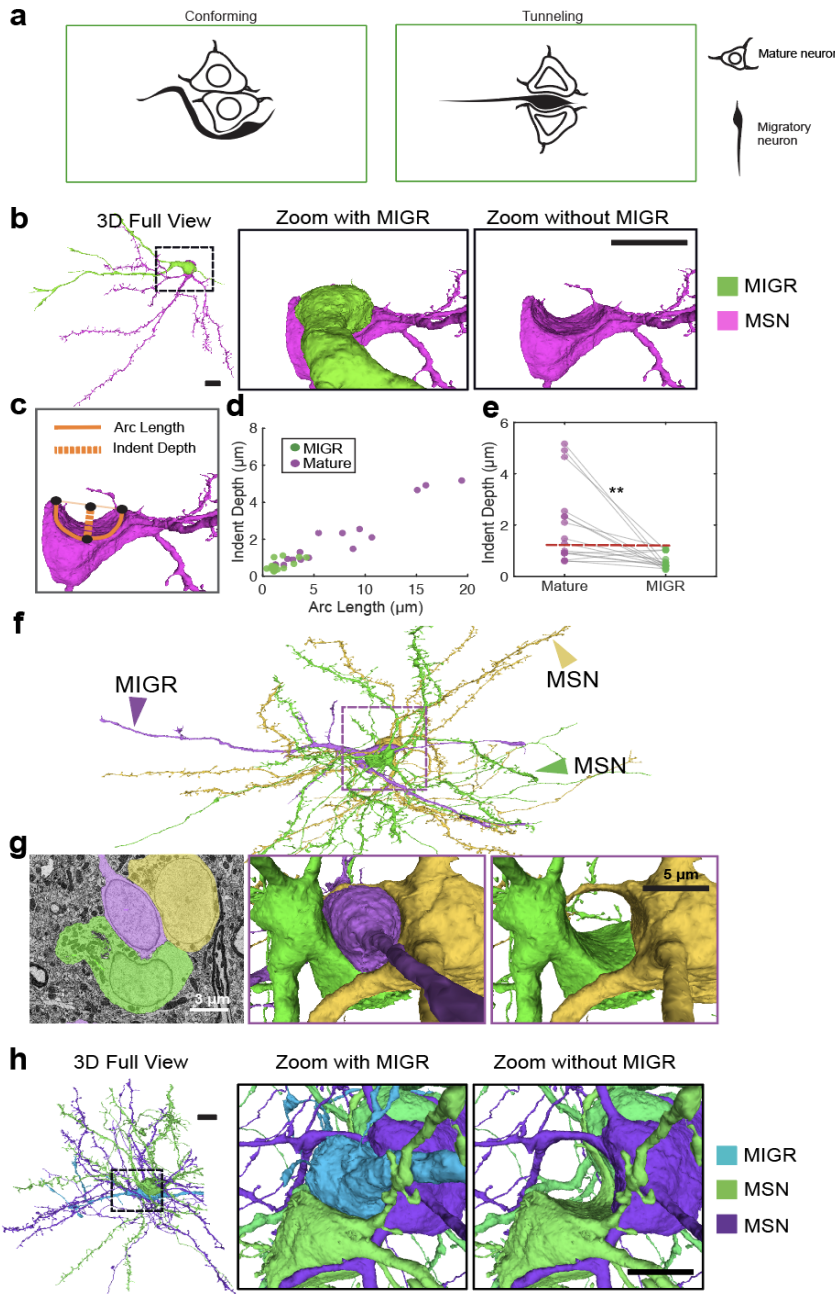
195 We next examined the interactions between new neurons and other classes of cells. In
196 other systems, many new neurons use scaffolds, such as radial fibers or blood vessels to migrate
197 ^{34,51}. However, we observed only a small minority of migratory neurons ($n = 8/35$) associated with
198 known migratory scaffolds (**Fig. S4**). In contrast, half of the identified migratory neurons formed
199 close soma-soma associations with mature neurons ($n = 17/35$ migratory neurons; **Fig. S4**) and,
200 to a lesser extent, astrocytes ($n=4/35$; **Fig. S5**). Interestingly, there was no significant difference
201 between the proximity of migratory neurons to mature neurons ($7.91 \mu\text{m} +/- 2.55 \mu\text{m}$) and the
202 proximity of random points throughout the volume to mature neurons ($9.14 \mu\text{m} +/- 4.00 \mu\text{m}$; KS
203 test: $p = 0.13$; **Fig. S4i,j**). Thus, these encounters may be due to the high density of mature
204 neurons along the paths of migrating neurons, rather than an active process of attraction or
205 avoidance.

206 Migratory neurons tunnel through the mature avian striatum

207 Given the prevalence of mature-migratory neuron soma contacts, we examined their
208 interactions in more detail. Specifically, we wondered whether migrating neurons conform their
209 shape to the boundaries of mature neurons (**Fig. 3a**). Examination revealed that, rather than
210 conforming to mature neurons, migrating neurons deformed adjacent neuron somas ($n = 17$
211 interactions; **Fig. 3b**).

212 To quantify this deformation we measured indentations at the site of contact between
213 migrating and mature neurons (**Fig. 3c**). These indents were large and asymmetrical between
214 contact partners (**Fig. 3d**). Indents were significantly deeper in mature neuron somas ($2.03 +/-$
215 $1.58 \mu\text{m}$ deep, $7.15 +/- 5.66 \mu\text{m}$ long) than in migratory neuron somas ($0.59 +/- 0.30 \mu\text{m}$ deep,
216 $1.64 +/- 1.08 \mu\text{m}$ long; paired t-test, $p < 0.004$; **Fig. 3e; Methods**). In several cases, migratory
217 neurons were found within large concavities through one or more mature neurons. This
218 phenomenon, in which new neurons appear to deform multiple adjacent neuron somas, axons,
219 and dendrites, we refer to as “tunneling.” Tunneling was particularly evident in migratory neuron
220 interactions with groups of densely packed mature neurons (**Fig. 3f-h**).

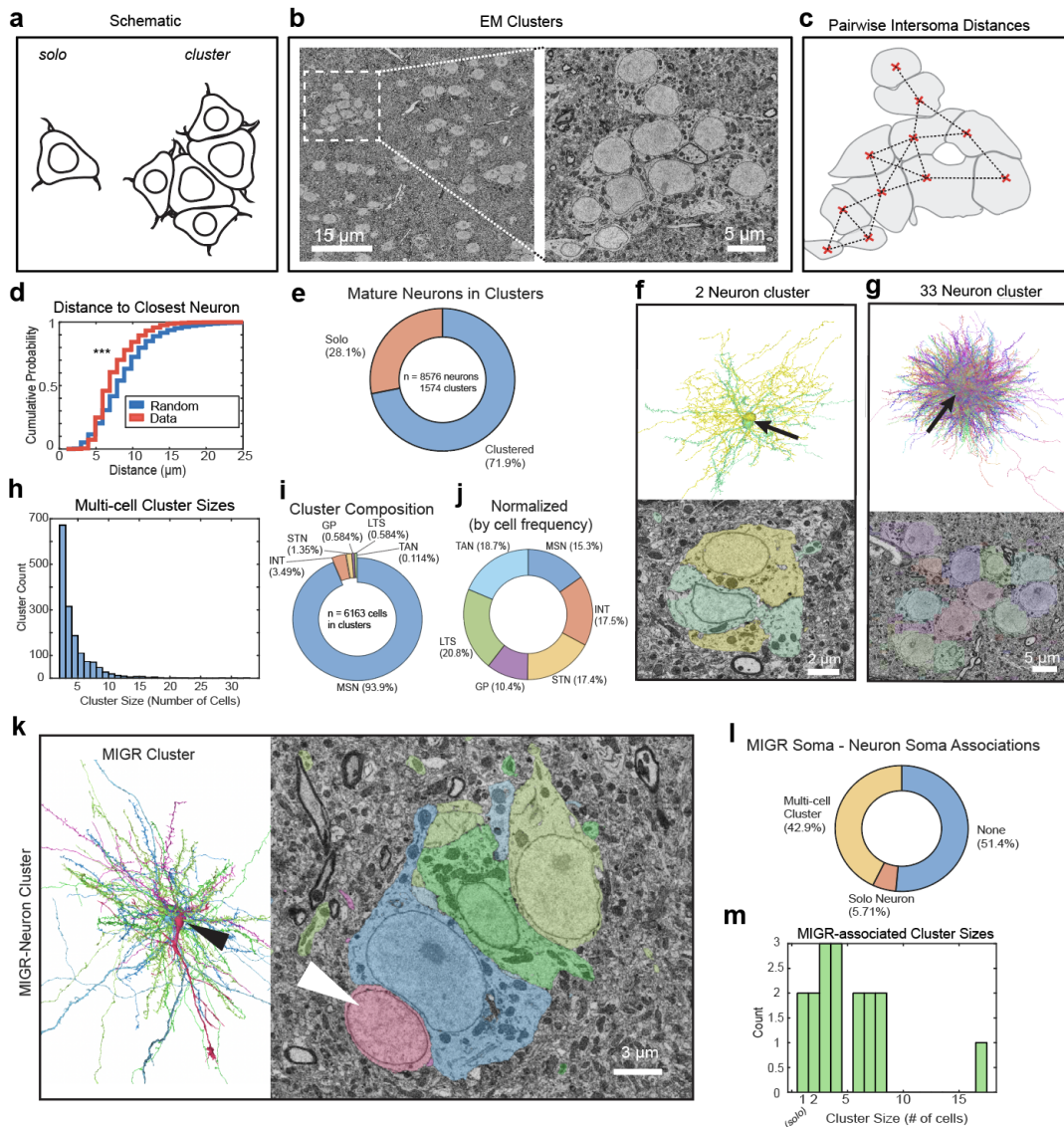
221 In the striatum, mature neurons were closer together than by chance (mean = $7.92 +/-$
222 $2.78 \mu\text{m}$; KS test, $p < 0.00001$) and frequently contacted the somas of other neurons (**Fig. 4**).
223 Similar dense groupings of mature neurons have been reported previously in other areas of the
224 avian brain where they have been called “clusters” ^{8,52-55}. We found that 71.9% of all mature
225 neurons ($n = 6163$) were found in clusters, defined as a connected graph of adjacent neuron
226 somas (minimum distance $<9 \mu\text{m}$ between soma centers, see **Methods**). Clusters ($n=1574$)
227 ranged in size from 2 to 33 neurons (mean = $4 +/- 3$) and contained all classes of mature neurons
228 (**Fig. 4e-h; Methods**) as well as glia (**Fig. S5**). The predominant cell type in the clusters were
229 MSNs ($n = 5786$ MSNs; 93.9% of all clustered cells; **Fig. 4i**), however, after normalization by cell
230 frequency, all neuron types had a similar contribution to cluster composition (**Fig. 4j**). New
231 neurons were found in clusters, where they indented one or more mature neurons forming tunnels
232 through the clusters (**Figure 4k-m**).



233 **Figure 3. Migratory neurons form indentations in mature neuron somas.**

234 A) Alternative strategies for interactions with mature somas. B) (*left*) Example 3D render of soma-soma
 235 contact between a migratory neuron (MIGR; green) and one MSN (pink). (*middle*) zoomed in perspective
 236 of MIGR and MSN, and (*right*) same zoom in perspective without the MIGR cell. Depth of indent is 2.15
 237 microns. Scale = 5 microns. C) Cell indent quantification method. D) Indent depth and length for each
 238 associated MIGR (green) and mature neuron (purple) ($n = 17$). E) Indent depth on each cell for MN-MIGR
 239 soma pairs ($n = 17$). Indent depth is significantly higher on mature neurons of each pair than their
 240 corresponding MIGR soma (paired t-test, $p < 0.004$). Red line indicates median mature neuron indent depth.
 241 F) Full 3D render of MIGR cell (purple) in soma-soma contact with two MSNs (yellow and green). G) (*left*)
 242 Electron micrograph of interaction from F. (*middle*) 3D render of MIGR cell (purple) and MSNs (green and
 243 yellow) from F. (*right*) 3D render of MSNs with MIGR cell removed. H) (*left*) “Tunneling” example with full
 244 view 3D rendering of MIGR (blue) and mature neurons (MSN class; green and purple), (*middle*) zoomed in

245 perspective of MIGR and MSNs, and (*right*) same perspective as in middle without MIGR. Depth of indent
 246 is 4.91 microns. Scale = 5 microns.



247 **Figure 4. Migratory neurons associate with neuronal clusters**
 248 A) Schematic of solo neuron vs cluster of neurons. B) Single plane EM micrograph from Area X. (*right*)
 249 zoomed in view of the dashed region. C) Schematic for intersomal distance quantification. Clusters were
 250 identified using nearest neighbor network analysis based on intersomal distance. D) Mature neurons (blue
 251 line) are closer to neuron neighbors than expected by chance (red line; KS test, $p < 0.00001$). E) Of all
 252 mature neurons, 28.1% are on their own, and 71.9% are in clusters. F) Example two neuron cluster. 3D
 253 render (top, arrow) and EM Micrograph (bottom). G) Example 33 neuron cluster, 3d render (top, arrow) and
 254 EM plane through somas (bottom). H) Distribution of computed cluster sizes. I)Cell type composition of all
 255 clusters. J) Cell type composition of all clusters, normalized by the frequency of each cell type in the data.
 256 K) Example migratory neuron (MIGR) associating with cluster. 3D renders (left) and EM micrograph (right).
 257 Arrowheads point to MIGR soma. L) Frequency of associations of MIGR cells with mature neuron somas.
 258 M) Sizes of clusters contacting migratory neurons.

259 Discussion

260 These data reveal the intricate interactions between migratory neurons in the adult
261 striatum and their local environment. Our findings support a model in which migrating neurons
262 disperse throughout dense neural tissue in multiple directions, making various contacts with
263 surrounding structures. In addition, our data reveal a previously undescribed form of neuron
264 migration in which new neurons cause deformities in nearby neurons and synapses. Together,
265 these data highlight the value of applying connectomics to problems in developmental
266 neuroscience^{56,57}.

267 Several features of the migration we observed resemble those reported in the embryonic
268 and adult nervous system, including in humans^{35,58–62}. However, to our knowledge, tunneling
269 migration by neurons has not previously been reported in the vertebrate nervous system. This
270 behavior contrasts with chain migration in the rostral migratory stream⁶³, where neurons move
271 through specialized corridors segregated from mature neurons, and with the amoeboid migratory
272 strategy observed in some glial cells, which typically conform to the contours of mature neuronal
273 somas⁶⁴. Interestingly, tunneling-like behavior has been described in metastatic cancer cells,
274 which navigate confined spaces by actively deforming their microenvironments⁶⁵. Tunneling may
275 therefore reflect a conserved strategy adopted by specialized migratory cell types in dense
276 tissues. Future research could uncover the molecular and biophysical mechanisms that may
277 enable this form of migration, and apply EM connectomics to evaluate its prevalence across
278 systems.

279 Importantly, tunneling reveals a potential cost of adult neuron migration—disruption of
280 existing circuits. As new neurons move through the mature tissues, mechanical disruption of cell
281 bodies, axons and dendrites could affect synaptic connections, either through breakage or acute
282 mechanical perturbation^{66–68}. Such perturbations could alter circuit-level dynamics and may
283 necessitate compensatory homeostatic mechanisms, similar to those proposed to support injury
284 resilience in the songbird brain^{69,70}. Alternatively, such network perturbations could also provide
285 a substrate for plasticity. Indeed, recent advances in deep reinforcement learning indicate that
286 sparse random perturbations in network connections can be used to facilitate continual learning
287 in artificial neural systems^{71,72}.

288 While the observed features are consistent with migratory identity, tunneling may reflect a
289 terminal stage of migration and may lead to the formation of neuron clusters. In other areas of the
290 songbird brain, new neurons preferentially integrate adjacent to mature ones^{8,30,52,73}, likely
291 benefiting from some local cues that support survival, maturation and integration^{54,55,74}. Future
292 studies using EM connectomics could illuminate these later stages, capturing how synaptic
293 contacts evolve as new neurons integrate into functional adult circuits.

294 Data availability

295 The dataset is available at SyConn Web (syconn.esc.mpcdf.mpg.de). All cells analyzed and used
296 in figures can be visualized with SyConn Web using the Cell IDs given in **Table S1**.

297 Ethics declarations

298 All authors declare no competing financial interests.

- 299 Acknowledgements
- 300 We thank Michale Fee, JoAnn Buchanan, Forrest Collman, and Maya Medalla for helpful
301 discussions. We thank Shawn Sorrells for comments on the manuscript. We thank the Boston
302 University Neurophotonics Center for funding, technical support, and imaging facilities. We also
303 acknowledge the Boston University Animal Science Center Staff for their care and maintenance
304 of the zebra finch colony, and we give a special acknowledgement to the sacrifice of the zebra
305 finches included in this work.
- 306 Author contributions
- 307 JK performed data collection, data curation and managed data sharing. BBS and JK conceived
308 the project. NRS, AR, SJC and DS performed analysis and contributed to figures. NRS wrote the
309 manuscript with feedback from BBS. All authors discussed and edited the manuscript.
310
- 311 References
- 312
- 313 1. Kempermann, G., Wiskott, L. & Gage, F. H. Functional significance of adult neurogenesis. *Curr. Opin. Neurobiol.* **14**, 186–191 (2004).
 - 314 2. Ming, G. & Song, H. Adult Neurogenesis in the Mammalian Brain: Significant Answers and
315 Significant Questions. *Neuron* **70**, 687–702 (2011).
 - 316 3. Chapouton, P., Jagasia, R. & Bally-Cuif, L. Adult neurogenesis in non-mammalian
317 vertebrates. *BioEssays* **29**, 745–757 (2007).
 - 318 4. Lehmenkühler, A., Syková, E., Svoboda, J., Zilles, K. & Nicholson, C. Extracellular space
319 parameters in the rat neocortex and subcortical white matter during postnatal development
320 determined by diffusion analysis. *Neuroscience* **55**, 339–351 (1993).
 - 321 5. Holtmaat, A., Wilbrecht, L., Knott, G. W., Welker, E. & Svoboda, K. Experience-dependent
322 and cell-type-specific spine growth in the neocortex. *Nature* **441**, 979–983 (2006).
 - 323 6. Roberts, T. F., Tschida, K. A., Klein, M. E. & Mooney, R. Rapid spine stabilization and
324 synaptic enhancement at the onset of behavioural learning. *Nature* **463**, 948–952 (2010).
 - 325 7. Alvarez-Buylla, A. & Nottebohm, F. Migration of young neurons in adult avian brain. *Nature*
326 **335**, 353–354 (1988).
 - 327 8. Kirn, J. R., Fishman, Y., Sasportas, K., Alvarez-Buylla, A. & Nottebohm, F. Fate of new
328 neurons in adult canary high vocal center during the first 30 days after their formation. *J.
329 Comp. Neurol.* **411**, 487–494 (1999).
 - 330 9. Goldman, S. A. & Nottebohm, F. Neuronal production, migration, and differentiation in a
331 vocal control nucleus of the adult female canary brain. *Proc. Natl. Acad. Sci.* **80**, 2390–2394
332 (1983).
 - 333 10. Paton, J. A. & Nottebohm, F. N. Neurons generated in the adult brain are recruited into
334 functional circuits. *Science* **225**, 1046–1048 (1984).
 - 335 11. Walton, C., Pariser, E. & Nottebohm, F. The Zebra Finch Paradox: Song Is Little Changed,
336 But Number of Neurons Doubles. *J. Neurosci.* **32**, 761–774 (2012).
 - 337 12. Alvarez-Buylla, A., Ling, C.-Y. & Yu, W. S. Contribution of neurons born during embryonic
338 and adult life to the brain of adult canaries: Regional specificity and delayed birth of neurons
339 in the song-control nuclei. *J. Comp. Neurol.* **347**, 233–248 (1994).
 - 340 13. Polomova, J., Lukacova, K., Bilcik, B. & Kubikova, L. Is neurogenesis in two songbird
341 species related to their song sequence variability? *Proc. R. Soc. B Biol. Sci.* **286**, 20182872
342 (2019).
 - 343 14. DeWulf, V. & Bottjer, S. W. Neurogenesis within the juvenile zebra finch telencephalic
344 ventricular zone: A map of proliferative activity. *J. Comp. Neurol.* **481**, 70–83 (2005).

- 346 15. Scott, B. B. & Lois, C. Developmental origin and identity of song system neurons born
347 during vocal learning in songbirds. *J. Comp. Neurol.* **502**, 202–214 (2007).
- 348 16. Puelles, L. et al. Pallial and subpallial derivatives in the embryonic chick and mouse
349 telencephalon, traced by the expression of the genes Dlx-2, Emx-1, Nkx-2.1, Pax-6, and
350 Tbr-1. *J. Comp. Neurol.* **424**, 409–438 (2000).
- 351 17. Rochefort, C., He, X., Scotto-Lomassese, S. & Scharff, C. Recruitment of FoxP2-expressing
352 neurons to area X varies during song development. *Dev. Neurobiol.* **67**, 809–817 (2007).
- 353 18. Kosubek-Langer, J., Schulze, L. & Scharff, C. Maturation, Behavioral Activation, and
354 Connectivity of Adult-Born Medium Spiny Neurons in a Striatal Song Nucleus. *Front.*
355 *Neurosci.* **11**, 323 (2017).
- 356 19. Kosubek-Langer, J. & Scharff, C. Dynamic FoxP2 levels in male zebra finches are linked to
357 morphology of adult-born Area X medium spiny neurons. *Sci. Rep.* **10**, 4787 (2020).
- 358 20. Arvidsson, A., Collin, T., Kirik, D., Kokaia, Z. & Lindvall, O. Neuronal replacement from
359 endogenous precursors in the adult brain after stroke. *Nat. Med.* **8**, 963–970 (2002).
- 360 21. Yamashita, T. et al. Subventricular Zone-Derived Neuroblasts Migrate and Differentiate into
361 Mature Neurons in the Post-Stroke Adult Striatum. *J. Neurosci.* **26**, 6627–6636 (2006).
- 362 22. Inta, D., Cameron, H. A. & Gass, P. New neurons in the adult striatum: from rodents to
363 humans. *Trends Neurosci.* **38**, 517–523 (2015).
- 364 23. Rother, A. et al., The Songbird Basal Ganglia Connectome, in preparation.
- 365 24. Schubert, P. J. et al. SyConn2: dense synaptic connectivity inference for volume electron
366 microscopy. *Nat. Methods* **19**, 1367–1370 (2022).
- 367 25. Shvedov, N. R. et al. In vivo imaging in transgenic songbirds reveals superdiffusive neuron
368 migration in the adult brain. *Cell Rep.* **43**, 113759 (2024).
- 369 26. Rao, M. S. & Shetty, A. K. Efficacy of doublecortin as a marker to analyse the absolute
370 number anddendritic growth of newly generated neurons in the adult dentate gyrus. *Eur. J.*
371 *Neurosci.* **19**, 234–246 (2004).
- 372 27. Balthazart, J., Boseret, G., Konkle, A. T. M., Hurley, L. L. & Ball, G. F. Doublecortin as a
373 marker of adult neuroplasticity in the canary song control nucleus HVC. *Eur. J. Neurosci.* **27**,
374 801–817 (2008).
- 375 28. Marusich, M. F., Furneaux, H. M., Henion, P. D. & Weston, J. A. Hu neuronal proteins are
376 expressed in proliferating neurogenic cells. *J. Neurobiol.* **25**, 143–155 (1994).
- 377 29. Barami, K., Iversen, K., Furneaux, H. & Goldman, S. A. Hu protein as an early marker of
378 neuronal phenotypic differentiation by subependymal zone cells of the adult songbird
379 forebrain. *J. Neurobiol.* **28**, 82–101 (1995).
- 380 30. Scott, B. B., Gardner, T., Ji, N., Fee, M. S. & Lois, C. Wandering Neuronal Migration in the
381 Postnatal Vertebrate Forebrain. *J. Neurosci.* **32**, 1436–1446 (2012).
- 382 31. Bellion, A. Nucleokinesis in Tangentially Migrating Neurons Comprises Two Alternating
383 Phases: Forward Migration of the Golgi/Centrosome Associated with Centrosome Splitting
384 and Myosin Contraction at the Rear. *J. Neurosci.* **25**, 5691–5699 (2005).
- 385 32. Kappeler, C. et al. Branching and nucleokinesis defects in migrating interneurons derived
386 from doublecortin knockout mice. *Hum. Mol. Genet.* **15**, 1387–1400 (2006).
- 387 33. Alvarez-Buylla, A., García-Verdugo, J. M., Mateo, A. S. & Merchant-Larios, H. Primary
388 Neural Precursors and Intermitotic Nuclear Migration in the Ventricular Zone of Adult
389 Canaries. *J. Neurosci.* **18**, 1020–1037 (1998).
- 390 34. Bovetti, S. et al. Blood Vessels Form a Scaffold for Neuroblast Migration in the Adult
391 Olfactory Bulb. *J. Neurosci.* **27**, 5976–5980 (2007).
- 392 35. Paredes, M. F. et al. Extensive migration of young neurons into the infant human frontal
393 lobe. *Science* **354**, aaf7073 (2016).
- 394 36. O'Rourke, N. A., Sullivan, D. P., Kaznowski, C. E., Jacobs, A. A. & McConnell, S. K.
395 Tangential migration of neurons in the developing cerebral cortex. *Dev. Camb. Engl.* **121**,
396 2165–2176 (1995).

- 397 37. Alderman, P. J. *et al.* Delayed maturation and migration of excitatory neurons in the juvenile
398 mouse paralaminar amygdala. *Neuron* **112**, 574–592.e10 (2024).
- 399 38. Matsumoto, M. *et al.* Dynamic Changes in Ultrastructure of the Primary Cilium in Migrating
400 Neuroblasts in the Postnatal Brain. *J. Neurosci.* **39**, 9967–9988 (2019).
- 401 39. Schaar, B. T. & McConnell, S. K. Cytoskeletal coordination during neuronal migration. *Proc.
402 Natl. Acad. Sci.* **102**, 13652–13657 (2005).
- 403 40. Yanagida, M., Miyoshi, R., Toyokuni, R., Zhu, Y. & Murakami, F. Dynamics of the leading
404 process, nucleus, and Golgi apparatus of migrating cortical interneurons in living mouse
405 embryos. *Proc. Natl. Acad. Sci. U. S. A.* **109**, 16737–16742 (2012).
- 406 41. Mascanzoni, F., Iannitti, R. & Colanzi, A. Functional Coordination among the Golgi
407 Complex, the Centrosome and the Microtubule Cytoskeleton during the Cell Cycle. *Cells* **11**,
408 354 (2022).
- 409 42. Nakazawa, N. & Kengaku, M. Mechanical Regulation of Nuclear Translocation in Migratory
410 Neurons. *Front. Cell Dev. Biol.* **8**, (2020).
- 411 43. Nakajima, C. *et al.* Identification of the growth cone as a probe and driver of neuronal
412 migration in the injured brain. *Nat. Commun.* **15**, 1877 (2024).
- 413 44. Chang, D. T. W. & Reynolds, I. J. Differences in mitochondrial movement and morphology in
414 young and mature primary cortical neurons in culture. *Neuroscience* **141**, 727–736 (2006).
- 415 45. Lin-Hendel, E. G., McManus, M. J., Wallace, D. C., Anderson, S. A. & Golden, J. A.
416 Differential Mitochondrial Requirements for Radially and Non-radially Migrating Cortical
417 Neurons: Implications for Mitochondrial Disorders. *Cell Rep.* **15**, 229–237 (2016).
- 418 46. Varum, S. *et al.* Energy Metabolism in Human Pluripotent Stem Cells and Their
419 Differentiated Counterparts. *PLoS ONE* **6**, e20914 (2011).
- 420 47. St John, J. C. *et al.* The expression of mitochondrial DNA transcription factors during early
421 cardiomyocyte in vitro differentiation from human embryonic stem cells. *Cloning Stem Cells*
422 **7**, 141–153 (2005).
- 423 48. Almeida, A. S. & Vieira, H. L. A. Role of Cell Metabolism and Mitochondrial Function During
424 Adult Neurogenesis. *Neurochem. Res.* **42**, 1787–1794 (2017).
- 425 49. Houghton, F. D. Energy metabolism of the inner cell mass and trophectoderm of the mouse
426 blastocyst. *Differ. Res. Biol. Divers.* **74**, 11–18 (2006).
- 427 50. Bertholet, A. M. *et al.* OPA1 loss of function affects in vitro neuronal maturation. *Brain J.
428 Neurol.* **136**, 1518–1533 (2013).
- 429 51. Alvarez-Buylla, A., Theelen, M. & Nottebohm, F. Mapping of radial glia and of a new cell
430 type in adult canary brain. *J. Neurosci.* **8**, 2707–2712 (1988).
- 431 52. Burd, G. D. & Nottebohm, F. Ultrastructural characterization of synaptic terminals formed on
432 newly generated neurons in a song control nucleus of the adult canary forebrain. *J. Comp.
433 Neurol.* **240**, 143–152 (1985).
- 434 53. Fortune, E. S. & Margoliash, D. Cytoarchitectonic organization and morphology of cells of
435 the field L complex in male zebra finches (*taenopygia guttata*). *J. Comp. Neurol.* **325**, 388–
436 404 (1992).
- 437 54. Gahr, M. & Garcia-Segura, L. M. Testosterone-dependent increase of gap-junctions in HVC
438 neurons of adult female canaries. *Brain Res.* **712**, 69–73 (1996).
- 439 55. Alcami, P. *et al.* Extensive GJD2 Expression in the Song Motor Pathway Reveals the Extent
440 of Electrical Synapses in the Songbird Brain. *Biology* **10**, 1099 (2021).
- 441 56. Gour, A. *et al.* Postnatal connectomic development of inhibition in mouse barrel cortex.
442 *Science* **371**, eabb4534 (2021).
- 443 57. Cordero Cervantes, D. *et al.* 3D reconstruction of the cerebellar germinal layer reveals
444 tunneling connections between developing granule cells. *Sci. Adv.* **9**, eadf3471 (2023).
- 445 58. Liang, Y. *et al.* Long-term in vivo single-cell tracking reveals the switch of migration patterns
446 in adult-born juxtaglomerular cells of the mouse olfactory bulb. *Cell Res.* **26**, 805–821
447 (2016).

- 448 59. Sorrells, S. F. *et al.* Immature excitatory neurons develop during adolescence in the human
449 amygdala. *Nat. Commun.* **10**, 2748 (2019).
- 450 60. Ang, E. S. B. C., Haydar, T. F., Gluncic, V. & Rakic, P. Four-dimensional migratory
451 coordinates of GABAergic interneurons in the developing mouse cortex. *J. Neurosci. Off. J.*
452 *Soc. Neurosci.* **23**, 5805–5815 (2003).
- 453 61. Inada, H. *et al.* GABA Regulates the Multidirectional Tangential Migration of GABAergic
454 Interneurons in Living Neonatal Mice. *PLOS ONE* **6**, e27048 (2011).
- 455 62. Tinterri, A. *et al.* Active intermixing of indirect and direct neurons builds the striatal mosaic.
456 *Nat. Commun.* **9**, 4725 (2018).
- 457 63. Lois, C., García-Verdugo, J.-M. & Alvarez-Buylla, A. Chain Migration of Neuronal
458 Precursors. *Science* **271**, 978–981 (1996).
- 459 64. Buchanan, J. *et al.* Oligodendrocyte precursor cells ingest axons in the mouse neocortex.
460 *Proc. Natl. Acad. Sci. U. S. A.* **119**, e2202580119 (2022).
- 461 65. Paul, C. D., Mistriotis, P. & Konstantopoulos, K. Cancer cell motility: lessons from migration
462 in confined spaces. *Nat. Rev. Cancer* **17**, 131–140 (2017).
- 463 66. Tyler, W. J. The mechanobiology of brain function. *Nat. Rev. Neurosci.* **13**, 867–878 (2012).
- 464 67. Kasuba, K. C. *et al.* Mechanical stimulation and electrophysiological monitoring at
465 subcellular resolution reveals differential mechanosensation of neurons within networks.
466 *Nat. Nanotechnol.* **19**, 825–833 (2024).
- 467 68. Cepkenovic, B., Friedland, F., Noetzel, E., Maybeck, V. & Offenhäusser, A. Single-neuron
468 mechanical perturbation evokes calcium plateaus that excite and modulate the network. *Sci.*
469 *Rep.* **13**, 20669 (2023).
- 470 69. Wang, B. *et al.* Unsupervised restoration of a complex learned behavior after large-scale
471 neuronal perturbation. *Nat. Neurosci.* **27**, 1176–1186 (2024).
- 472 70. Duffy, A., Abe, E., Perkel, D. J. & Fairhall, A. L. Variation in sequence dynamics improves
473 maintenance of stereotyped behavior in an example from bird song. *Proc. Natl. Acad. Sci.*
474 **116**, 9592–9597 (2019).
- 475 71. Dalm, S., Gerven, M. van & Ahmad, N. Effective Learning with Node Perturbation in Multi-
476 Layer Neural Networks. Preprint at <https://doi.org/10.48550/arXiv.2310.00965> (2025).
- 477 72. D’Oro, P. *et al.* Sample-Efficient Reinforcement Learning by Breaking the Replay Ratio
478 Barrier. in (2022).
- 479 73. Alvarez-Buylla, A. & Kirn, J. R. Birth, migration, incorporation, and death of vocal control
480 neurons in adult songbirds. *J. Neurobiol.* **33**, 585–601 (1997).
- 481 74. Ikeda, M. Z., Jeon, S. D., Cowell, R. A. & Remage-Healey, L. Norepinephrine Modulates
482 Coding of Complex Vocalizations in the Songbird Auditory Cortex Independent of Local
483 Neuroestrogen Synthesis. *J. Neurosci.* **35**, 9356–9368 (2015).
- 484 75. Agate, R. J., Scott, B. B., Haripal, B., Lois, C. & Nottebohm, F. Transgenic songbirds offer
485 an opportunity to develop a genetic model for vocal learning. *Proc. Natl. Acad. Sci. U. S. A.*
486 **106**, 17963–17967 (2009).
- 487 76. Januszewski, M. *et al.* High-precision automated reconstruction of neurons with flood-filling
488 networks. *Nat. Methods* **15**, 605–610 (2018).
- 489 77. Dorkenwald, S. *et al.* Automated synaptic connectivity inference for volume electron
490 microscopy. *Nat. Methods* **14**, 435–442 (2017).

491
492
493
494
495
496
497
498

499
500
501

Supplementary Materials

for

502 Songbird connectome reveals tunneling of migratory neurons in 503 the adult striatum

504

505 Shvedov, N.R., Castonguay, S.J., Rother, A., Schick, D.E., Kornfeld, J., Scott, B.B.*

506 *Correspondence to: bbs@bu.edu

507

508

509 Includes:

510

511 Methods

512 Figs. S1 to S6

513 Table S1

514 Supplementary References

515 Methods

516 Immunohistochemistry

517 Animal use procedures were approved by the Boston University Institutional Animal Care
518 and Use Committee (IACUC; Protocol #201800577) and carried out in accordance with National
519 Institutes of Health standards. Birds were housed under standard conditions (12h/12h light/dark
520 cycle).

521 Transgenic UBC-GFP transgenics^{1,2} were bred at Boston University. Adult male zebra
522 finches were euthanized with Euthasol (Virbac) and perfused with up to 20 mL of 1X phosphate-
523 buffered saline (PBS), followed by up to 50 mL of 10% neutral buffered formalin. The brain was
524 extracted and stored in formalin overnight. After fixation, the brain was washed with PBS and
525 sliced into 40 or 50 µm sections with a vibratome (Leica; VT1000S).

526 The primary antibodies used were a mouse monoclonal anti-DCX (1:300 dilution) (Santa
527 Cruz Biotechnology, sc-271390 (E-6), lot: C3121)³. We also stained with a mouse monoclonal
528 anti-HuC/HuD that is a marker for cells in neuronal lineage in 1:250 dilution (ThermoFisher
529 Scientific A-21271)⁴. The secondary antibodies used were Alexa Fluor 568 conjugated goat anti-
530 mouse (Invitrogen) in a 1:500 dilution.

531 Antigen retrieval was performed prior to staining by incubating slices in a 50 mM solution
532 of Tris buffer (Fisher Scientific) at a pH of 8.4 for 30 min. Then, tissue sections were placed in a
533 blocking solution composed of 2% nonfat dry milk, 0.02% Triton X-100 (Sigma), and 1X PBS.
534 Sections were incubated at 4°C overnight in primary antibody diluted in blocking solution, washed
535 3 times with PBS, then incubated with secondary antibody diluted in blocking solution for 1 h at
536 room temperature or overnight at 4°C. Sections were mounted on microscope slides (Fisher
537 Scientific) using Vectashield Antifade Mounting Medium with DAPI (Vector Laboratories, Inc.).

538 Histological fluorescent images from striatal nucleus Area X were acquired using a confocal
539 microscope (Zeiss LSM800, Germany). Image processing was performed with FIJI/ImageJ.

540 Machine learning based identification of migratory neurons

541 Ground truth cells ($n=14$) were manually selected from the zebra finch Area X
542 connectome⁵ using morphological characteristics shared with fluorescent imaging data identifying
543 migratory neuron morphology. These cells were used to train a supervised learning algorithm,
544 based on previous methods^{6–8}. The IDs for these cells were: 751594441, 971410555,
545 2157811112, 38332384, 1773210639, 328158994, 1644151292, 561503453, 1104854425,
546 28511657, 2656656549, 669941616, 763200873, 245868794.

547 This approach returned 135 objects which were manually inspected. 40/135 exhibited
548 morphological and ultrastructural features consistent with migratory neurons. This data indicate a
549 false positive rate of 79.4%.

550 To evaluate the false negative rate, i.e. migratory neurons that were missed by the
551 algorithm, we visually inspected a set of >2,000 low-confidence (< 0.5 certainty) medium spiny
552 neurons and microglia, possessing a segment volume between 460 and 1500 μm^3 , and < 200
553 identified synapses. Using this method we identified 28 cells with morphology and ultrastructure
554 features consistent with migratory neurons. All 28 cells found through a manual algorithm were
555 found within these 40, indicating an undetectable false negative rate. If cells were drastically
556 clipped, or had no distinct leading process (5/40), they were excluded from further analysis.

557 Cell orientation analysis

558 To determine the orientation vectors of each cell, three X, Y, Z coordinates were extracted
559 in the Syconn Neuroglancer interface. The three coordinates corresponded to the start of the
560 soma (a_{XYZ} ; at the base of the leading process), the first bifurcation point of the leading process
561 (b_{XYZ}), and the distal tip of the leading process (c_{XYZ} ; **Fig. S3a,b**). All further analyses were
562 performed in Matlab using a custom script.

563 The orientation of the cell was determined by the direction of the vector between a_{XYZ} and
564 b_{XYZ} and the magnitude of the vector (only used for plotting in **Fig. S3c,d**) was determined by the
565 approximate length of the cell from a_{XYZ} to c_{XYZ} .

566 After the orientation vector was extracted ($b_{XYZ} - a_{XYZ}$), it was normalized by dividing the
567 vector by its Euclidean norm (using the *norm* Matlab function) to make the value of each
568 dimension (in X, Y, and Z) its relative contribution to the overall orientation (maximum value of 1
569 in any dimension). If all cells were pointed in the same direction, the magnitude of their averaged
570 orientation vector would be 1. This was to account for differences in physical length between the
571 soma and bifurcation point of all cells which should not contribute to the overall orientation
572 estimates.

573 Mitochondrial density estimates

574 Mitochondria were segmented and annotated previously⁷. For cell IDs that were filtered
575 and verified above, the summed volume of all mitochondria voxels was divided by each
576 segmented cell's volume to yield the total mitochondrial volume density ($\mu\text{m}^3/\mu\text{m}^3$). A one-way
577 ANOVA was performed to test for significant differences in mitochondrial density across groups.

578 Synapse density estimates

579 Synapses were segmented and annotated previously using automated methods^{7,8}. Only
580 synapses with a classifier certainty greater than or equal to 0.90 were used for analysis in Matlab.
581 For local density estimates around migratory neurons (MIGR), all synapses within a 10 µm search
582 radius from the MIGR soma center coordinate (n = 35 MIGR somas) were counted and divided
583 by the search volume (20 µm x 20 µm x 20 µm) to yield the local synapse density in µm⁻³ for each
584 cell. For local synapse density around random points, the local synapse density was computed
585 around every micron voxel throughout the data (n = 29484).

586 Shannon Entropy estimation

587 Shannon entropy of actual data (soma and synapse positions) or simulated data was
588 computed as described previously¹. Briefly, the three-dimensional volume containing the positions
589 was binned into different sized bins, and we computed the probability of containing a data point
590 for each 3-dimensional bin. We then input these probabilities into the Shannon entropy formula:

$$591 \quad Entropy = -\sum p(S_b) * \log(p(S_b))$$

592

593 where $p(S_b)$ is the probability that a soma's or synapse's position is within any spatial bin. We
594 repeated this process while we increased the bin sizes and plotted the entropy across bin sizes.

595 Cell somas and cluster analysis

596 Soma positions were extracted from segmented objects with several predicted
597 compartments. Only cells that had a soma compartment, as well as dendrites and an axon that
598 were at least 200 µm in skeleton path length were selected. All cell types other than MSN and
599 INT were then manually verified and any segmented cells that were merged with another fragment
600 or cell were removed from analysis. For MSN and INT, a random subset of cells was verified
601 manually. The median of the soma vertex coordinates was used as the "soma center." Three-
602 dimensional coordinates from each segmented soma were then analyzed in Matlab (n = 8576
603 neurons).

604 To find the nearest neighbor of all mature neurons, pairwise distance calculations were
605 performed between each soma center coordinate. The minimum pairwise distance for each cell
606 was considered the distance to its nearest neighbor. A similar analysis was performed for MIGR
607 cells for which the cell soma center was determined manually in the SyConn Neuroglancer
608 interface. Then, the minimum pairwise distance between MIGR and all other mature neurons was
609 extracted to find the distance to the nearest neighbor. The minimum distance found between a
610 MIGR soma center and a mature neuron soma center was 2.575 µm.

611 For "random" distances, we created a binary three-dimensional matrix where the position
612 of each soma center coordinate was a "1". Then, we performed a distance transform on this binary
613 3D soma matrix to find distance between every element and the nearest nonzero element.
614 Distances below 2.575 were determined to be biologically improbable and were removed.

615 For an analysis of cluster size and composition, a graph-based connected components
616 approach was taken. First, a distance transform on the binary 3D matrix of soma positions was
617 performed. The resultant matrix contained the 3D distance between each element and every other
618 nonzero element. We next iteratively determined an appropriate distance threshold, 9 µm
619 (approximately double the average soma radius of 4.46 µm) to find cells belonging to the same

620 cluster. After testing several distance thresholds ranging from 8 to 11 μm , we found that 9 μm
621 yielded no false positives in the largest output clusters. However, using this approach, we
622 detected a nonzero false negative rate, suggesting we are underrepresenting cluster sizes with
623 this analysis.

624 Then, we applied this threshold to the distance matrix so that every value greater than 9
625 μm became zero, and cells that were clustered together below this distance threshold were
626 represented as groups of ones. Using Matlab's conncomp function, connected components
627 composed of singular groups of ones were found and stored in structs as separate clusters. The
628 cell IDs belonging to these clusters were extracted and visualized in the Syconn Neuroglancer
629 interface to confirm accurate cluster identification with this algorithm. Cluster sizes were computed
630 from the data and cluster compositions were extracted.

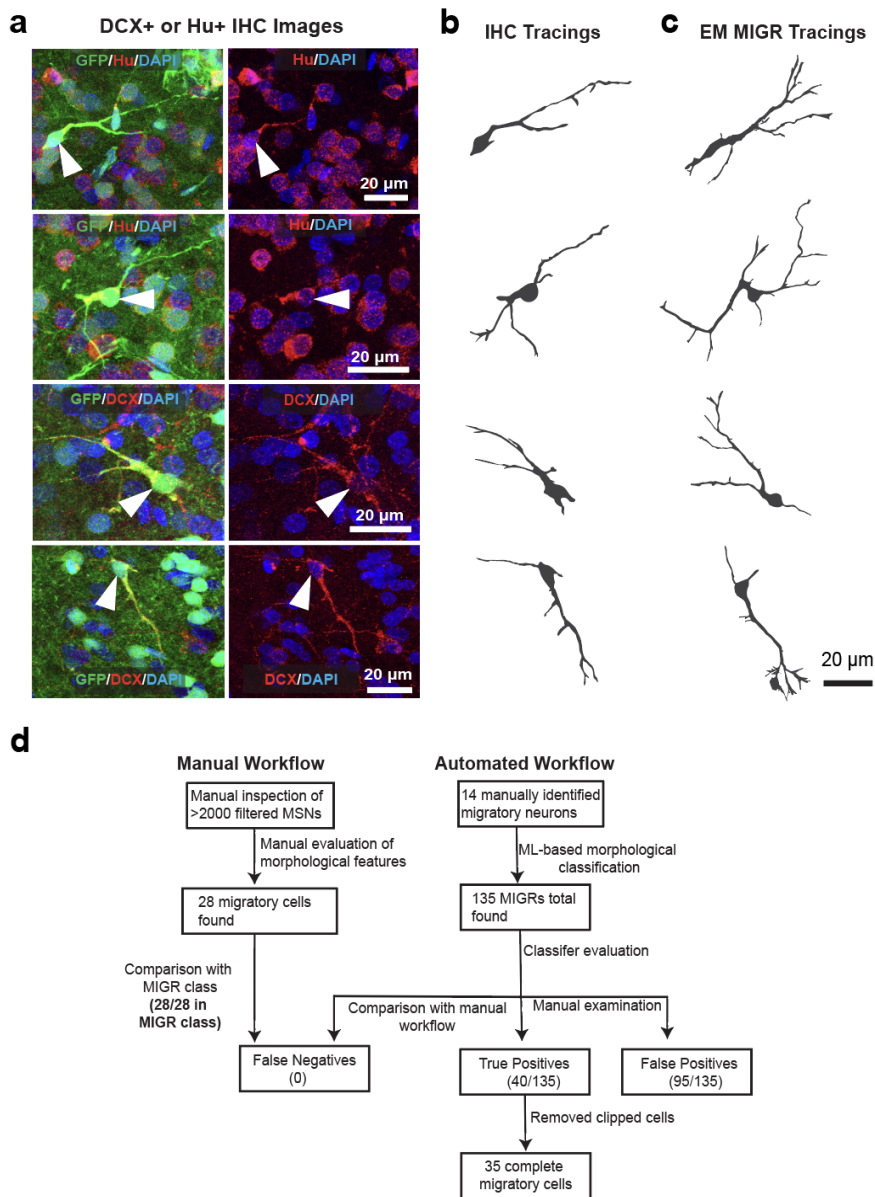
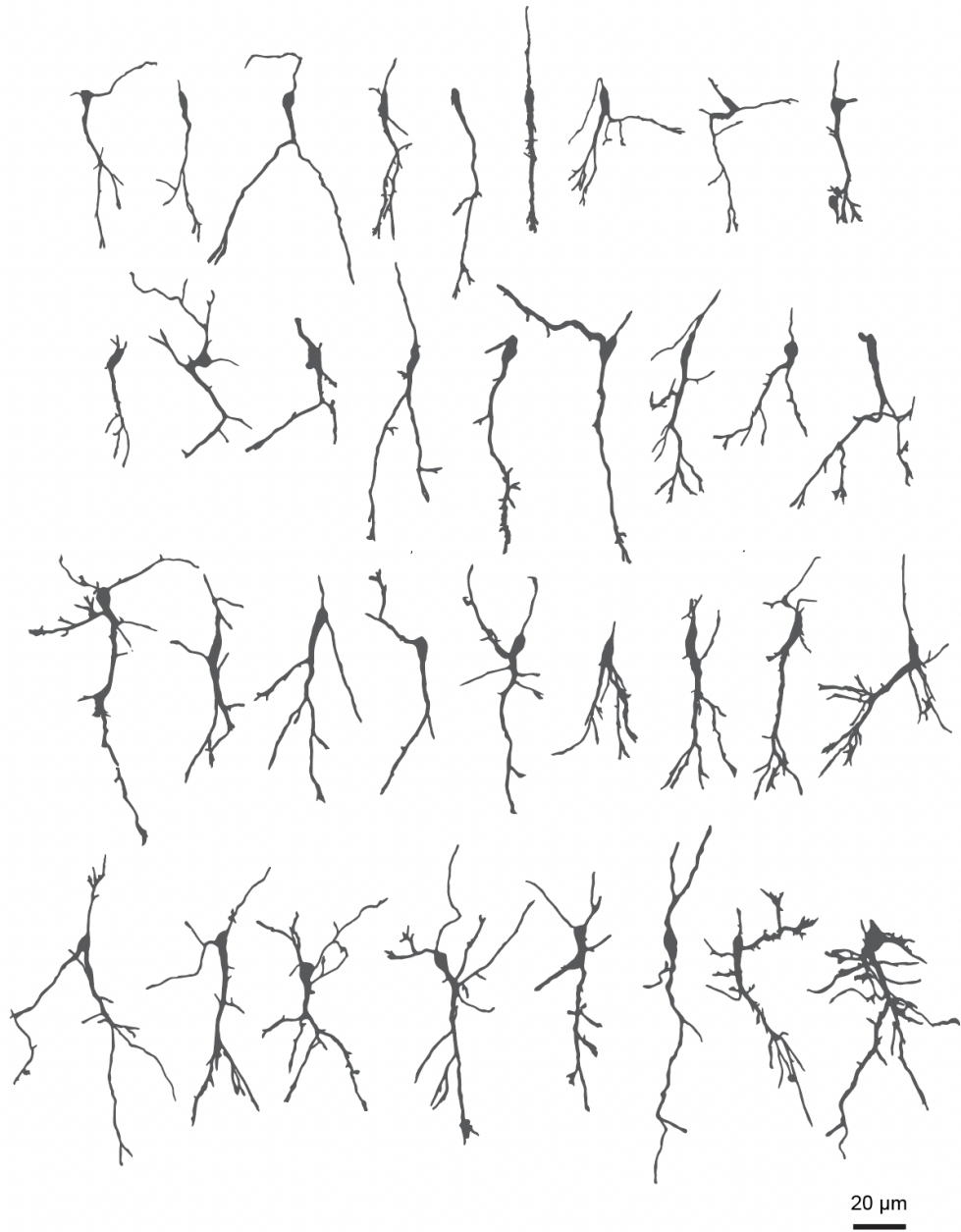


Figure S1. Workflow for identification of migratory neurons in EM

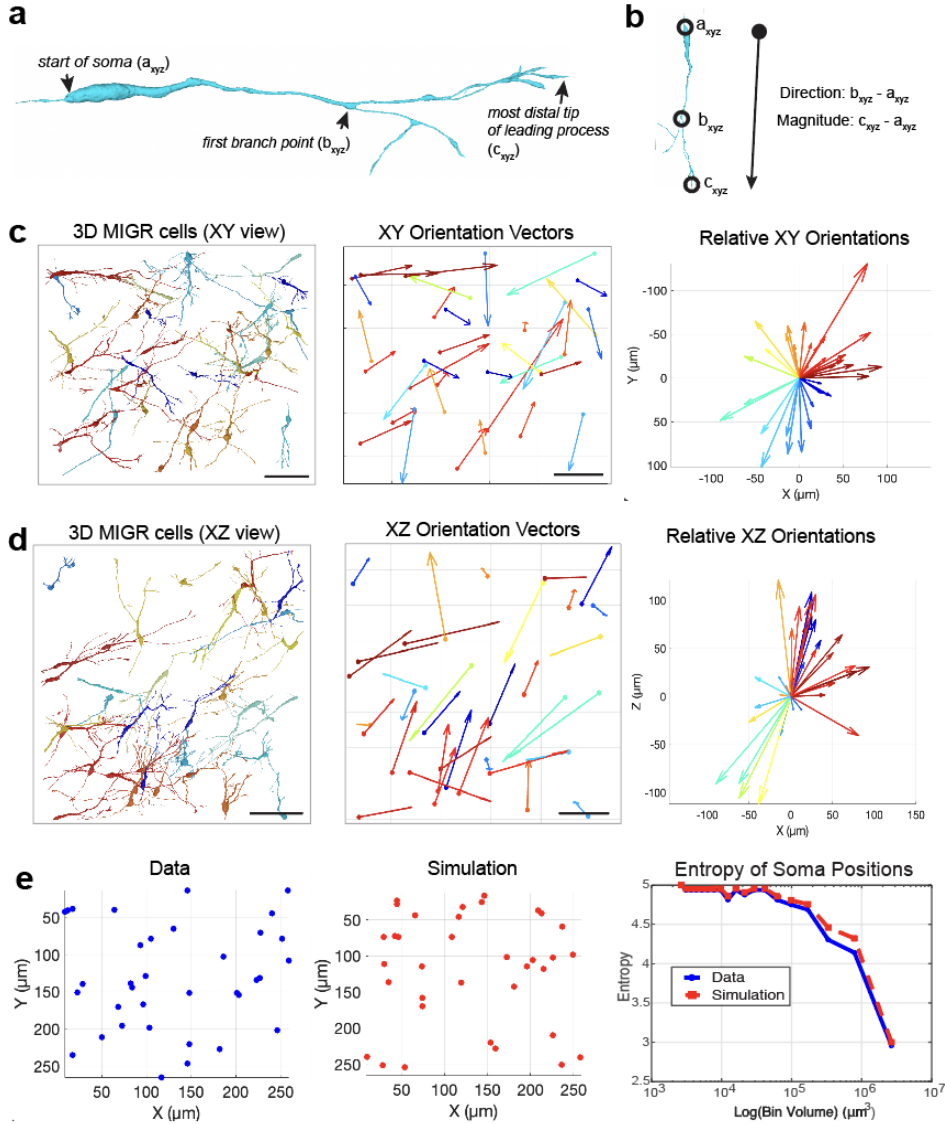
A) Confocal images of histological sections from UBC-GFP transgenic birds. Sections are labeled with immunohistochemistry against GFP (green) and either DCX (red, upper two panels) or HU (red, lower panels). Co-stained cells with a migratory morphology are indicated with an white arrow. B) Tracings of cells from A. C) Reconstructions of cells with similar morphology from the songbird connectome. D) Two workflows were used to identify migratory cells in the songbird connectome: manual (left) and automated (right). In the manual workflow, expert human observers inspected hundreds of reconstructions to identify cells that met the morphological criteria of migrating neurons. In the automated workflow, 14 manually identified cells were used to train a convolutional neural network-based classifier. The trained classifier resulted in the construction of a cell class with 135 objects. The manual workflow was then used to assess the false negative rate of the automated approach.



643

644

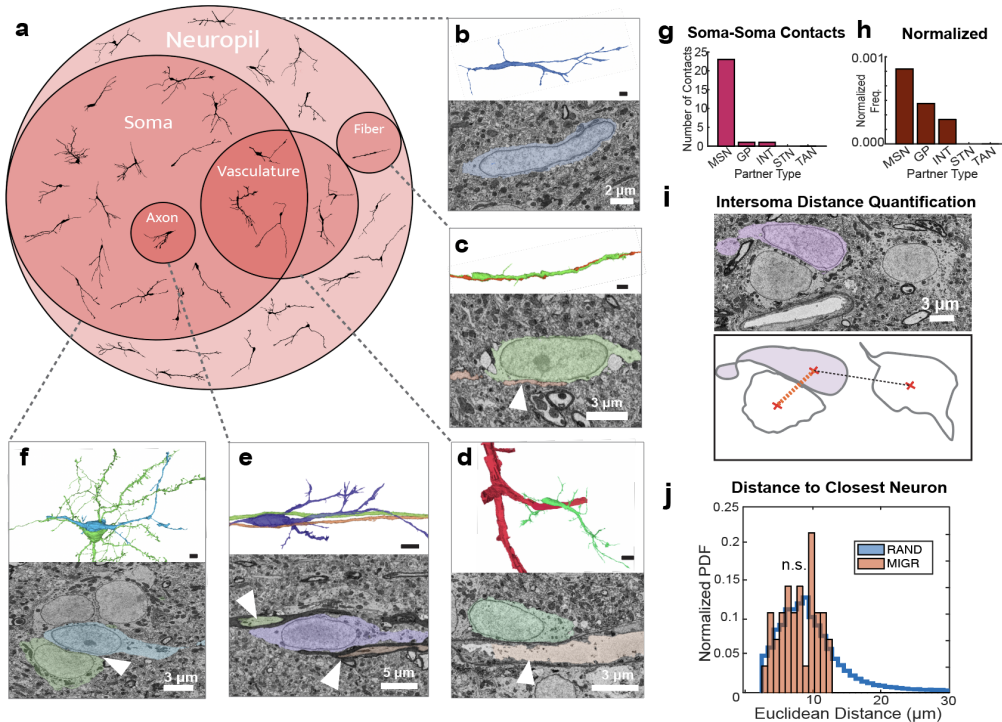
645 **Figure S2. Morphology of identified migratory cells.** Cells with migratory neuron morphology and
646 ultrastructure ordered by volume. Note cells vary in complexity; most possess branched leading processes.
647



648
649
650 Figure S3. Migratory neurons are widely distributed and oriented in multiple directions
651
652
653
654
655
656
657
658
659
660
661

- A. Morphological features used for computing cell orientation.
- B. Formula for computing cell orientation.
- C. Left: XY view of migratory neurons (MIGR; n=35) in the volume. Middle: XY orientation vectors; magnitude of vectors vary according to length of MIGR. Scale bars: 50 microns. Right: Polar plot of relative XY vector directions with start position and magnitude normalized. No directional bias was detected (Rayleigh's test, p = 0.05).
- D. Left: XZ view of MIGR cells (n=35). Middle: MIGR XZ orientation vectors; Right: Polar plot of relative XZ vector directions. Significant directional bias was detected (Rayleigh's test, p < 0.001).
- E. Left: Recorded soma positions. Middle: Simulated soma positions (maximum entropy model). Right: Computed entropy of data (blue) vs simulation (red) across different bin sizes.

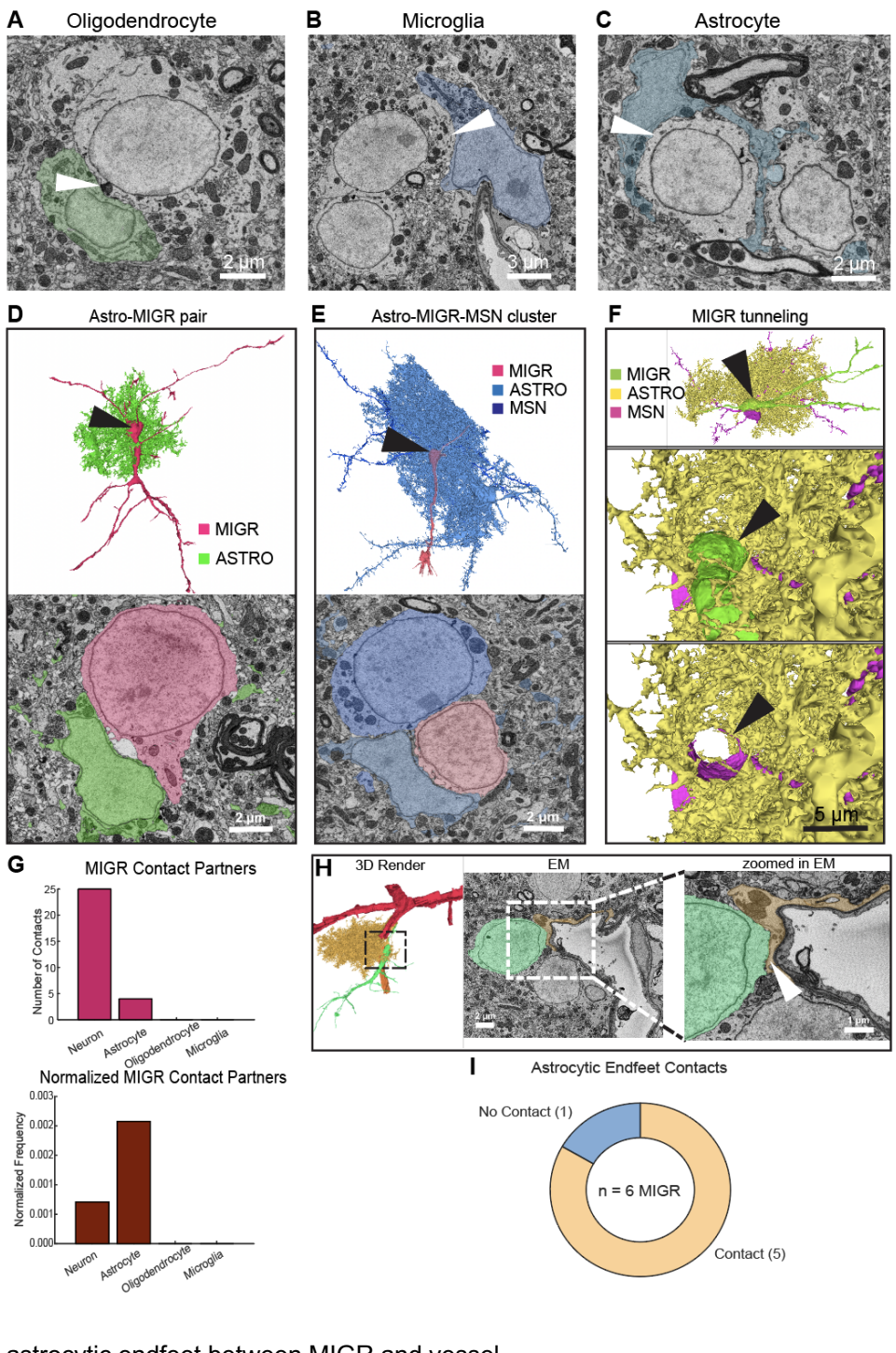
662
663

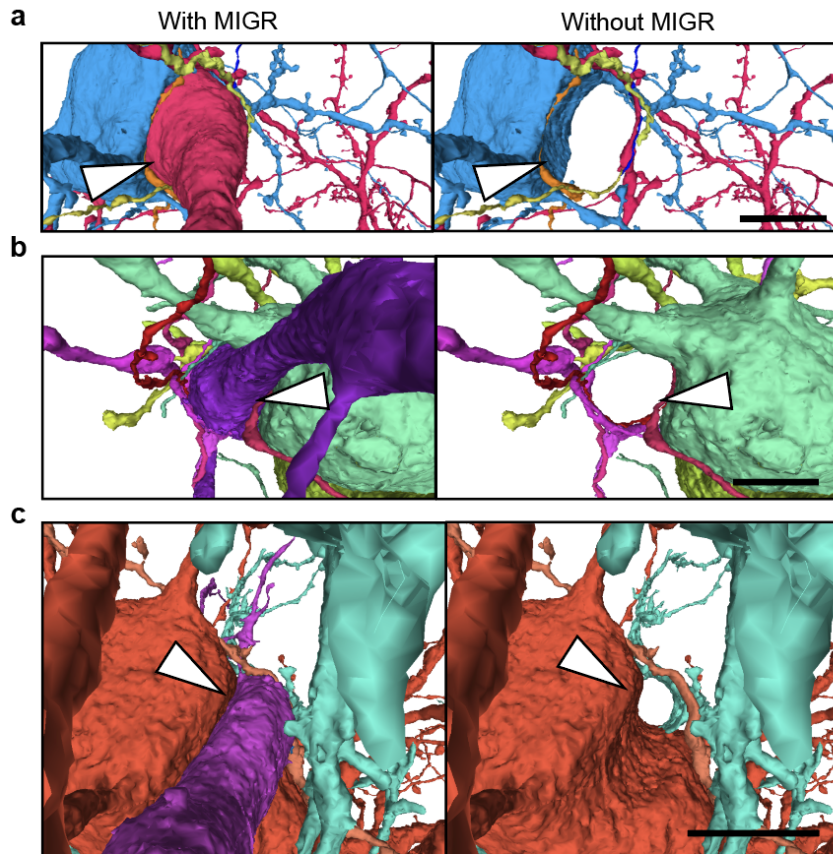


664 **Figure S4. Migratory cells contact a variety of mature cell types**
665 a) Partners for migratory cells: We evaluated the contacts of all migratory neurons to test if they associate
666 with a particular type of structure known to be a cellular scaffold for migration. We manually inspected the
667 microenvironment surrounding the somas of migratory neurons in three dimensions and recorded adjacent
668 cells and structures with significant membrane contact as determined by manual inspection.. Circle size
669 represents the number of migratory cells (shown in black) that make contact with a particular structure.
670 Overlapping circles indicate cells with multiple contact partners for cells in the intersecting region.
671 b) Example migratory neuron (MIGR) found in neuropil with no observable soma-soma contacts nor fibers
672 closely aligned with the cell soma.
673 c-f) Example cells with contact partners shown as a 3D rendering (top) and color-coded 2D electron
674 micrograph (bottom). Contact partners include fibers [c], vasculature (f), axons (e), mature neurons somas (f)
675 g) Frequency of MIGR soma contacts with other neuron types.
676 h) Normalized frequency of MIGR soma contacts with multiple neuron types.
677 i) Method of quantification of intersoma distances between MIGR cells and mature neurons. Red X's denote
678 the 3D center coordinate for each soma, and the dashed lines represent 3D distance. Orange dashed line is
679 the minimum intersoma distance.
680 j) Computed distances of random points (RAND; blue) to nearest mature soma center, and distances of 35
681 MIGR soma centers to nearest mature soma center (MIGR; orange). No significant difference in distribution
682 (KS test, $p = 0.15$).

683 **Fig. S5 Glial interactions with mature and migratory neurons**

684 A-C) Example soma-soma
 685 interaction between
 686 oligodendrocytes (A), microglia
 687 (B) and Astrocytes (C) and
 688 medium spiny neurons (MSNs).
 689 Arrowhead points to the
 690 deformation of the glia soma
 691 membrane.
 692 D) Soma-soma interaction
 693 between migratory neuron (MIGR)
 694 and astrocyte. 3D render (top)
 695 with an arrow pointing to somas
 696 portrayed in EM micrograph
 697 (bottom).
 698 E) MIGR cell part of a soma
 699 cluster containing an MSN and an
 700 astrocyte. 3D render (top) with an
 701 arrow pointing to somas portrayed
 702 in EM micrograph (bottom).
 703 F) Example of MIGR tunnel
 704 through MSN and astrocyte
 705 cluster. Top panel shows zoom
 706 out 3D render with arrowhead
 707 pointing to MIGR soma. Middle
 708 panel shows zoom in view of
 709 soma interaction between all cells.
 710 Bottom panel shows same view
 711 as middle without the MIGR cell.
 712 G) (top) Bar plot of MIGR soma
 713 contacts with neurons and
 714 different glial types. (bottom)
 715 Normalized by cell frequency.
 716 H) (left) 3D render of MIGR cell
 717 contacting portion of blood vessel.
 718 (middle) EM micrograph of MIGR
 719 soma contact with blood vessel.
 720 Zoom in on dashed box from
 721 middle. White arrowhead points to
 722 astrocytic endfeet between MIGR
 723 soma and endothelial cells of
 724 vessel.
 725 I) Proportion of MIGRs that contact astrocytic endfeet between MIGR and vessel.
 726
 727





728

729

730

731

732

733

734

735

Figure S6 Tunneling examples. Each row is a zoom in on migratory neuron (MIGR) soma interaction with surrounding neurons or neuropil. Left column has MIGR rendered, right column is the same view shown without the MIGR cell. White arrowhead points to MIGR soma position. MIGR IDs from panels a - c, respectively, are 1977673147, 299547481, 1711566114, and 2732540650. Scale is 5 μ m.

736

737

MIGR ID	Figure Panel	
28511657	1d	739
38332384	-	740
751594441	-	741
1017028811	-	742
1644151292	1g	744
2157811112	-	745
2732540650	3h	746
76319964	-	747
971410555	2b,c,d	748
1542156551	-	749
245868794	-	750
1677253391	-	751
1711566114	2i,j,k	752
299547481	-	753
2657431890	-	754
1773210639	-	755
68425094	3b	756
328158994	-	757
763200873	-	758
1849326393	-	759
1104854425	-	760
1850337533	-	761
232640459	-	762
728009703	-	763
1368397294	1f	764
561503453	-	765
669941616	-	766
624562902	-	767
261826889	-	768
2003753184	-	769
82666072	-	770
197685997	-	771
420403179	-	772
282311177	3f,g	773
1977673147	4k	774

775

Table S1. Table of identified migratory neurons. ID numbers of the 35 complete migratory cells (MIGR) and associated main figure panel. All of the cells are depicted in Fig. 1b.

776

777

778 Supplementary References

- 779
- 780 1. Shvedov, N. R. *et al.* In vivo imaging in transgenic songbirds reveals superdiffusive neuron
781 migration in the adult brain. *Cell Rep.* **43**, 113759 (2024).
- 782 2. Agate, R. J., Scott, B. B., Haripal, B., Lois, C. & Nottebohm, F. Transgenic songbirds offer
783 an opportunity to develop a genetic model for vocal learning. *Proc. Natl. Acad. Sci. U. S. A.*
784 **106**, 17963–17967 (2009).
- 785 3. Balthazart, J., Boseret, G., Konkle, A. T. M., Hurley, L. L. & Ball, G. F. Doublecortin as a
786 marker of adult neuroplasticity in the canary song control nucleus HVC. *Eur. J. Neurosci.* **27**,
787 801–817 (2008).
- 788 4. Barami, K., Iversen, K., Furneaux, H. & Goldman, S. A. Hu protein as an early marker of
789 neuronal phenotypic differentiation by subependymal zone cells of the adult songbird
790 forebrain. *J. Neurobiol.* **28**, 82–101 (1995).
- 791 5. Rother, A. *et al.*, The Songbird Basal Ganglia Connectome, in preparation.
- 792 6. Januszewski, M. *et al.* High-precision automated reconstruction of neurons with flood-filling
793 networks. *Nat. Methods* **15**, 605–610 (2018).
- 794 7. Schubert, P. J. *et al.* SyConn2: dense synaptic connectivity inference for volume electron
795 microscopy. *Nat. Methods* **19**, 1367–1370 (2022).
- 796 8. Dorkenwald, S. *et al.* Automated synaptic connectivity inference for volume electron
797 microscopy. *Nat. Methods* **14**, 435–442 (2017).
- 798
- 799
- 800